Journal of ELECTRONIC MATERIALS, Vol. 49, No. 1, 2020
https://doi.org/10.1007/s11664-019-07703-8


# Enhancing the Properties of Spark Plasma Sintered Nanocrystalline NdFeB Magnets by the Addition of Cu-Zn Alloy and $Dy_2O_3$ Powders

SHENGLONG HU,[1] JING LIU,[1] YUKUN LIU,[1] JIASHENG ZHANG,[2] HONGYA YU,[2] KUNPENG SU,[3] YOULIN HUANG,[4] and ZHONGWU LIU[2,5]

1.—School of Automotive Studies, Jiangxi College of Applied Technology, Ganzhou 341000, People's Republic of China. 2.—School of Material Science and Engineering, South China University of Technology, Guangzhou 510640, People's Republic of China. 3.—School of Materials and Environmental Engineering, Hangzhou Dianzi University, Hangzhou 310012, People's Republic of China. 4.—School of Material Science and Engineering, Nanchang Hangkong University, Nanchang 330063, People's Republic of China. 5.—e-mail: zwliu@scut.edu.cn

Nanocrystalline NdFeB bulk magnets were synthesized by doping non-rare earth $Cu_xZn_{100-x}$ ($x$ = 0, 10, and 60 wt.%) alloy powders and low-cost $Dy_2O_3$ powders into melt-spun $Nd_{10.15}Pr_{1.86}Fe_{80.41}Al_{1.67}B_{5.91}$ powders using spark plasma sintering (SPS). Their microstructure and magnetic properties were systematically studied. The results indicate that in the magnets doped with 1.0 wt.% $Cu_{10}Zn_{90}$ powders, Cu or Zn is evenly partitioned in irregular particle interfaces, which can improve the densification during SPS due to the "connection" effect. Zn or $Dy_2O_3$ plays an important role in suppressing grain coarsening of the $Nd_2Fe_{14}B$ phase during SPS. Doping with 0.5 wt.% Zn, 0.5 wt.% $Cu_{10}Zn_{90}$ or 0.1 wt.% $Cu_{60}Zn_{40}$ powders can effectively improve the magnetic properties of the final products, and their intrinsic coercivities ($_jH_c$) are about 11.3%, 15.6%, 11.7% higher, respectively, than that of the additive-free magnet. Meanwhile, the SPS magnets doped with 0.5 wt.% Zn or 0.5 wt.% $Cu_{10}Zn_{90}$ powders show high $_jH_c$ values with slight increases in both remanent magnetic polarization $J_r$ and maximum energy product $(BH)_{max}$. The magnets doped with both 0.1 wt.% $Cu_{60}Zn_{40}$ and 1.0 wt.% $Dy_2O_3$ powders exhibit the highest $_jH_c$ of 1630 kA/m.

**Key words:** Nanocrystalline NdFeB, Cu-Zn alloy powders, $Dy_2O_3$ powders, spark plasma sintering, regular/irregular interface

## INTRODUCTION

NdFeB sintered magnets have been used in various applications, and they have contributed to reducing the size and improving the performance of hybrid electric vehicles (HEV), electric vehicles (EV), magnetic resonance imaging (MRI) units, etc. For those used at relatively high temperature, both high remanence and high coercivity are required.[1,2]

In 2006, Hirota et al.[2] reported an alternative process, called the *grain boundary diffusion process* (GBDP), to enhance the intrinsic coercivity $_jH_c$ of NdFeB magnets without a drastic reduction of $J_r$ and $(BH)_{max}$. Since then, this process has been developed quickly. For a typical GBDP, Dy or other heavy rare earth (HRE) elements in the form of oxide, fluoride or pure metal is firstly coated on the NdFeB magnets and a subsequent diffusion heat treatment is employed to modify the microstructure.[3–6] Recently, Huang et al.[7] also showed that magnets with $_jH_c$ of 1184 kA/m and maximum energy product $(BH)_{max}$ of 238 kJ/m$^3$ could be obtained by grain boundary diffusion of a non-rare earth (Al). However, the

(Received April 23, 2019; accepted September 28, 2019; published online October 11, 2019)

limited diffusion depth, approximately 5 mm in maximum from the surface to the center, seriously restricts the application of this approach.

Alternatively, doping a non-rare earth metal is a practical method to enhance the properties of NdFeB magnets. Compared with the GBDP, this method is much simpler and easier to realize. First, mix the additives evenly with the NdFeB powders before sintering. At present, the reported additives are mainly focused on the rare earth-containing or non-rare earth element powders, for example, oxides[8] and fluorides[9–11] of Nd or Dy, non-rare earth elements such as Zn,[8,12] Al[12] or Sn.[12] Doping non-rare earth binary alloys such as Cu-Zn, has not been well investigated.

Meanwhile, spark plasma sintering (SPS) is a comparatively new sintering technique for preparing nanocrystalline NdFeB magnets. It allows very fast heating and cooling rates, very short holding time, and the possibility to obtain fully dense samples at comparatively low sintering temperatures, typically a few hundred degrees lower than the traditional hot-pressing process. A wide variety of materials, e.g., ceramics, composites, metals and alloys, have been successfully compacted by the SPS process.[13–22] For NdFeB magnets, it is well known that refining the grain size is an effective method to improve the value of $_jH_c$, which indicates that SPS technology is a good choice for preparing high performance nanocrystalline NdFeB permanent magnets.

In this work, to obtain the NdFeB magnets with high performance, both the advantages of SPS and traditional doping have been taken into account. Specifically, the effect of doping non-rare earth $Cu_xZn_{100-x}$ alloy powders and low-cost $Dy_2O_3$ powders into sintered NdFeB magnets are studied systematically.

## EXPERIMENTAL

Commercial melt-spun powders with a nominal composition of $Nd_{10.15}Pr_{1.86}Fe_{80.41}Al_{1.67}B_{5.91}$ (at.%) with particle size up to 200 $\mu$m and grain size $< 100$ nm were used as the starting materials. The magnetic powders were mixed evenly with $Cu_xZn_{100-x}$ ($x$ = 0, 10, and 60 wt.%) powders or $Cu_xZn_{100-x}$ and $Dy_2O_3$ powders in a high-purity Ar atmosphere. The average particle sizes of $Cu_xZn_{100-x}$ and $Dy_2O_3$ powders are $\sim$ 9 and 3 $\mu$m, respectively. The isotropic bulk magnets were prepared by SPS using an SPS-825 machine (Sojitz Machinery Corporation). The powders were heated from room temperature to 1023 K in 600 s, and then were consolidated at this temperature for 300 s with a pressure of 60 MPa. The typical SPS samples have a cylindrical shape with a diameter of 20 mm and a height of about 7–10 mm.

The phase constitution was characterized by a Philips X'Pert diffractometer using Cu-$K_\alpha$ radiation. For microstructure characterization, the sintered magnets were violently broken and the fresh fractures were observed by scanning electronic microscopy (Nano430, FEI Company). The element distributions in the magnets were studied by means of line-scan and plane-scan using an energy dispersive spectrometer (EDS). For EDS analysis, considering that the shape of the pores changes during polishing and small pores may even be closed afterward, a relatively flat fresh fracture area without polishing was selected directly to carry out the experiment. The magnetic properties of the samples were measured using a Physical Property Measurement System (PPMS-9, Quantum Design, USA) equipped with a 9 T vibrating sample magnetometer (VSM). The densities of the magnets were measured based on the Archimedes principle.

## RESULTS AND DISCUSSION

Figure 1 shows the XRD patterns of sintered magnets doped with Zn powders with different weight ratios. The phase structure has no

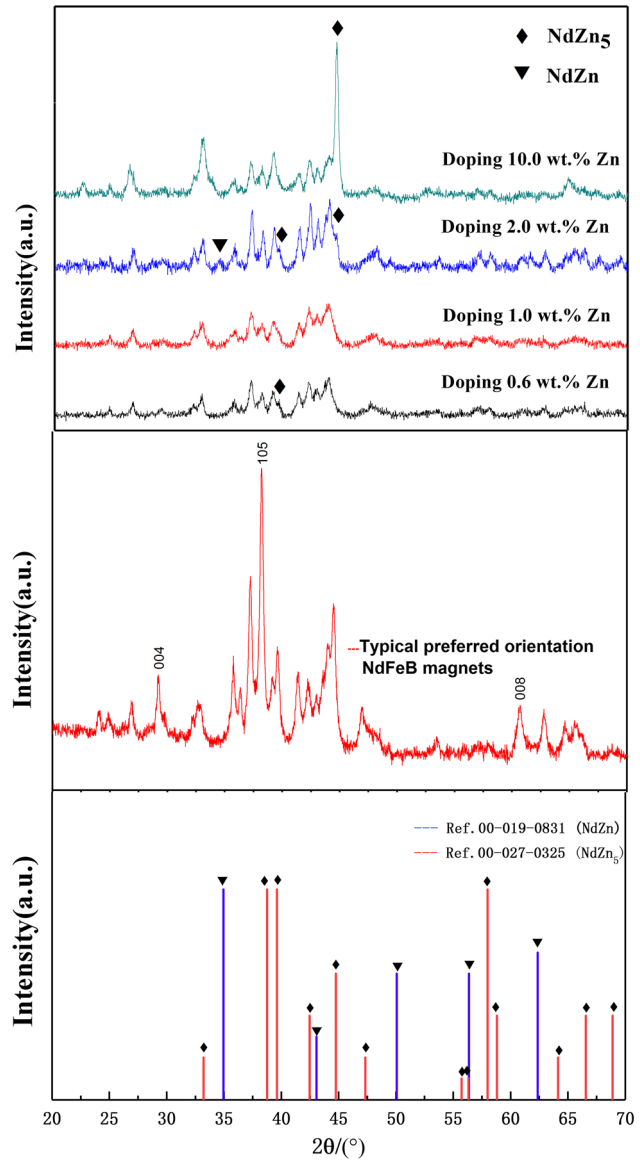


Fig. 1. XRD patterns of sintered magnets doped with Zn powders with different weight ratios.

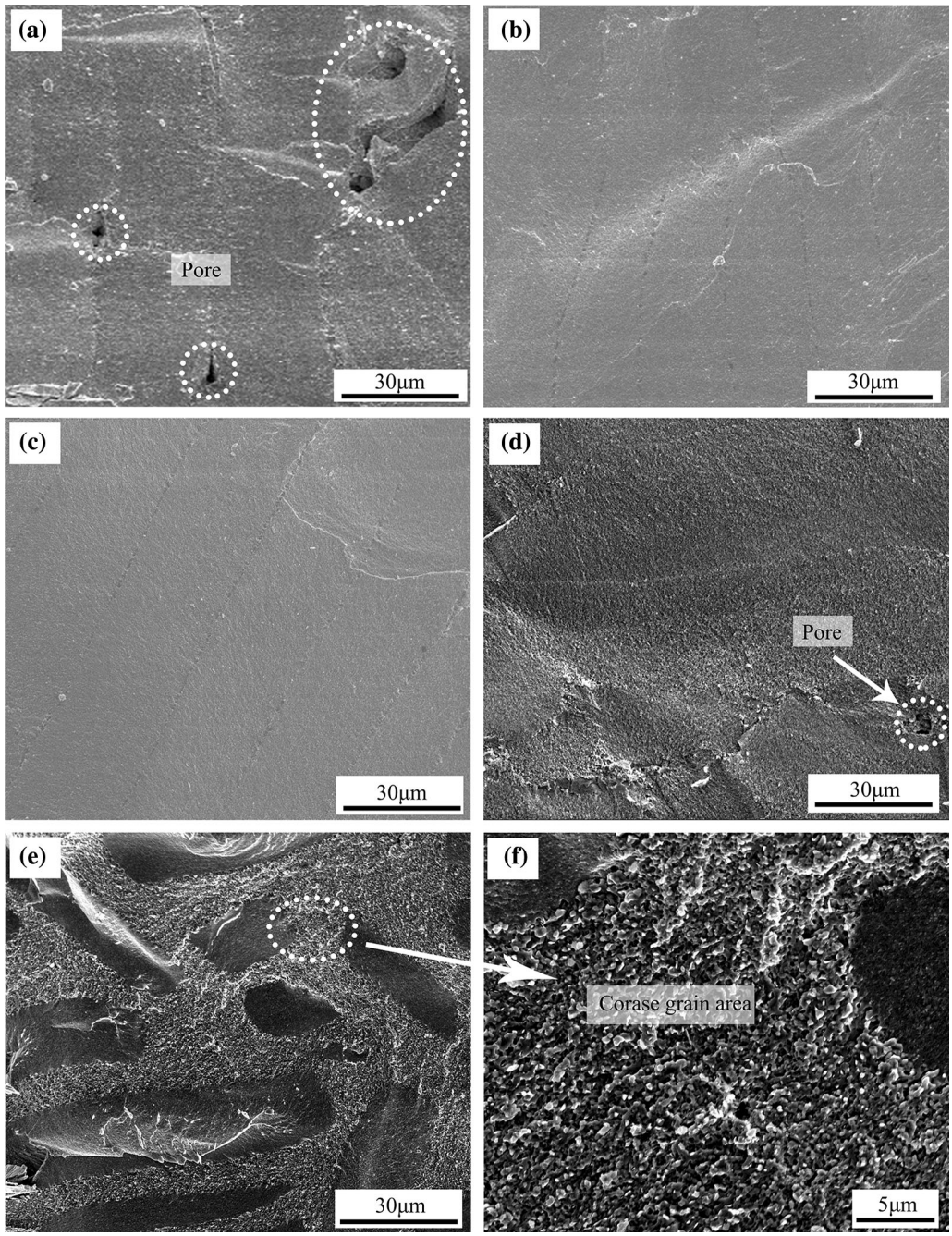


Fig. 2. SEM images for the sintered magnets with various $Cu_xZn_{100-x}$ additions: (a) Additive-free, (b) 0.5 wt.% Zn, (c) 0.5 wt.% $Cu_{10}Zn_{90}$, (d) 0.1 wt.% $Cu_{60}Zn_{40}$, (e) 10.0 wt.% Zn, (f) amplified figure of (e).

significant change after SPS. Compared with the typical anisotropic NdFeB magnet shown in XRD patterns, there are no preferred orientation diffraction peaks [(0 0 4)/(1 0 5)/(0 0 8)] observed, indicating that anisotropy not formed after SPS. In addition, only trace amount of NdZn phase was detected in the magnet doped with 0.6 wt.% Zn and no new phase was found in the magnet doped with 1.0 wt.% Zn, which can be attributed to the low content of additives. By increasing the Zn content to 2.0 wt.% and 10.0 wt.%, NdZn and $NdZn_5$ phases were observed in Zn-doped magnets, implying that Zn can react with the Nd-containing phase in melt-spun powders to form Nd-Zn compounds, and the NdZn phase will gradually transform into the $NdZn_5$ phase with increasing Zn content. It is considered that the combined effect between $NdZn_5$ and $Nd_2Fe_{14}B$ phases is responsible for the higher peak intensity at $2\theta$ of 44.8° for the magnets doped with 10.0 wt.% Zn powders.

Figure 2 shows the SEM images for the sintered magnets doped with various $Cu_xZn_{100-x}$ alloy powders ($x$ = 0, 10, and 60 wt.%). Some micro-pores were observed in additive-free samples, as shown in Fig. 2a. Comparing the different samples, doping 0.5 wt.% Zn or 0.5 wt.% $Cu_{10}Zn_{90}$ powders can effectively decrease the amount of micro-pores. Zn or Cu-Zn alloy powders plays an important role in the formation of fully dense magnets during SPS, as shown in Fig. 2b and c. Micro-pores were also observed in the samples doped with $Cu_{60}Zn_{40}$ powders, as shown in Fig. 2d, which may be attributed to the relatively lower conductivity and higher melting point of the $Cu_{60}Zn_{40}$ alloy than Zn or $Cu_{10}Zn_{90}$ alloy. Meanwhile, the sintered magnets doped with a high content of $Cu_xZn_{100-x}$ ($x$ = 0) alloy powders were also prepared and their microstructures are shown in Fig. 2e and f. For the sintered magnets doped with 10.0 wt.% Zn powders, a large amount of coarse grains appear in the magnet, which is not beneficial for the magnet's properties.[23,24]

Considering the variations in the size and morphology of starting powders, both regular particle interface and irregular particle interface can be

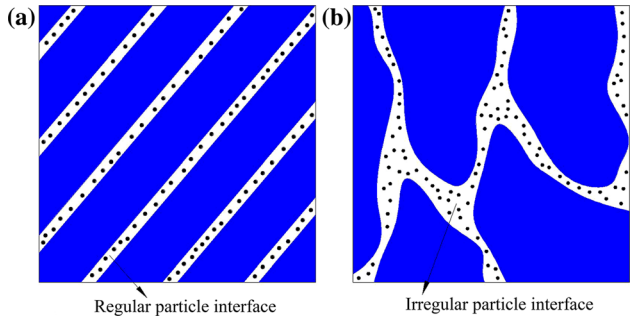


Fig. 3. The schematic of (a) regular particle interface and (b) irregular particle interface in green compacts of the powders before SPS (the blue regions are the inside of the powder, the white regions are the particle interface, the black dots are doping powders) (Color figure online).

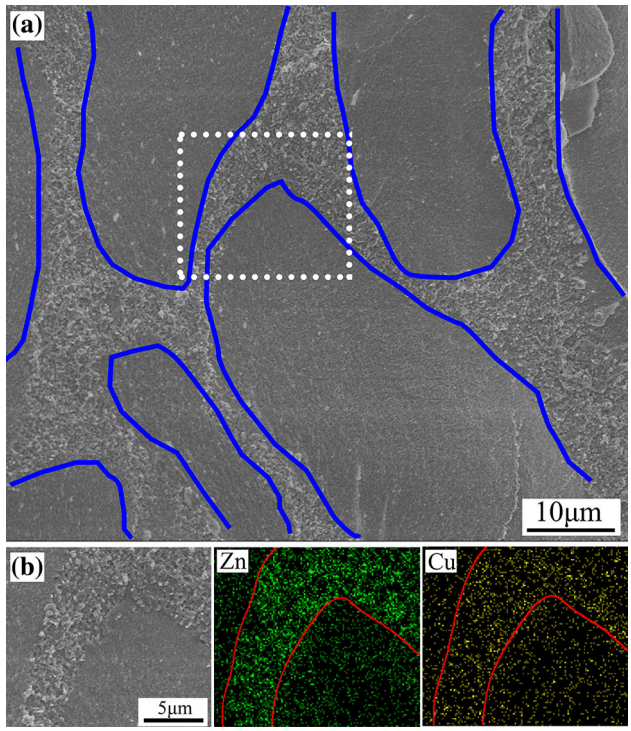


Fig. 5. Typical microstructure (a) and the selected area (b) with the plane-scan profiles of Zn and Cu in the irregular particle interface for the magnet doped with 1.0 wt.% $Cu_{10}Zn_{90}$ alloy powders.

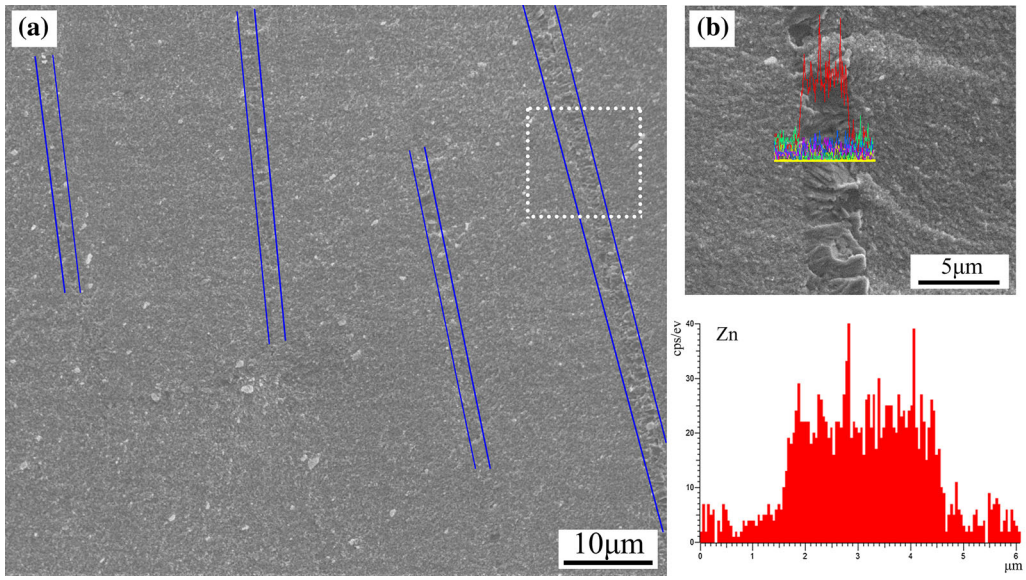


Fig. 4. Typical microstructure (a) and the selected area (b) with a line-scan profile of Zn across the regular particle interface along the yellow horizontal line for the magnet doped with 1.0 wt.% Zn powders (Color figure online).

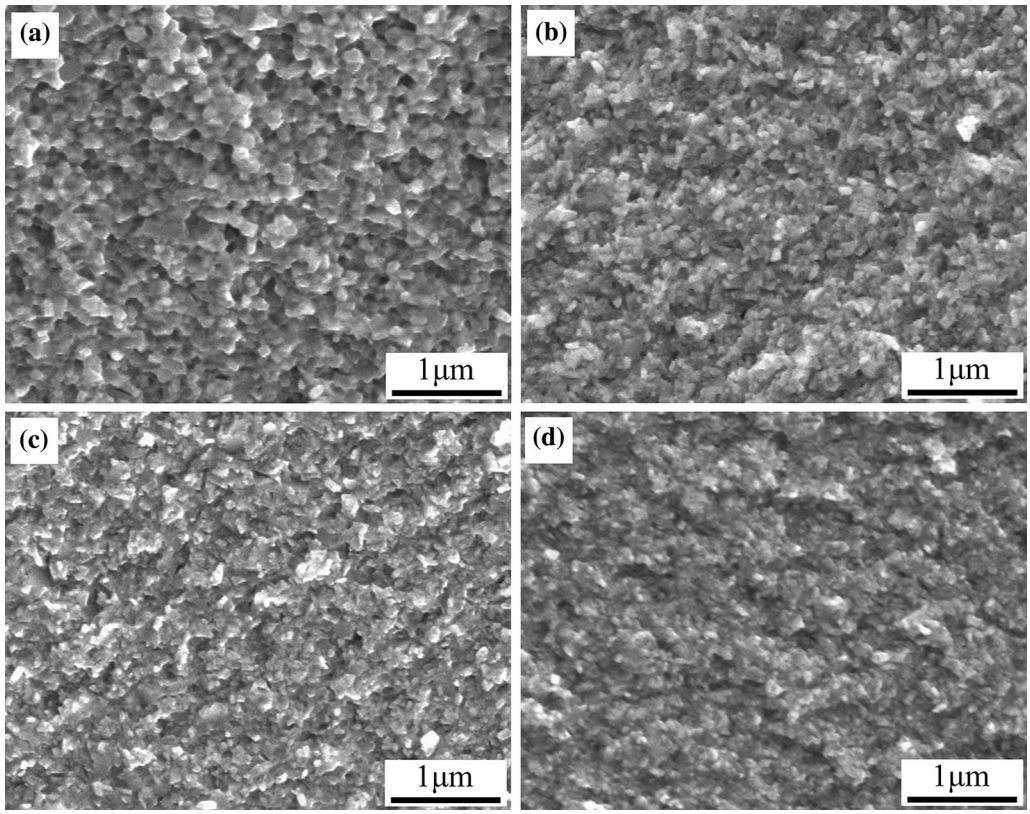


Fig. 6. The grain morphology of areas away from interface for the sintered magnets doped with different powder additions: (a) Additive-free; (b) 0.6 wt.% Zn; (c) 2.0 wt.% $Dy_2O_3$. (d) 0.6 wt.% Zn + 2.0 wt.% $Dy_2O_3$.

formed in green compact, which can be explained using the schematic shown in Fig. 3. For the regular particle interface in green compacts, as shown in Fig. 3a, the particle interface should be "connected" in a straight line during SPS for evenly distributed interface gaps. The low-melting point of Cu-Zn alloy powders may help to further decrease the amount of micro-pore during SPS by the "connection" effect. For the irregular particle interface in green compacts, however, it is reasonable to consider that fully dense magnets cannot be prepared due to the unevenly gap distributions, as shown in Fig. 3b. If the gaps among the irregular particles can be filled by doped low-melting alloy powders, the excessive gaps may be "connected" successfully during SPS.

Zn or Cu distributions in the particle interface were also investigated. Figure 4 illustrates the line-scan profile of Zn across the regular particle interface along the yellow horizontal line shown in Fig. 4b for the magnets doped with 1.0 wt.% Zn powders. Figure 5 presents the plane-scan profiles of Zn and Cu in the irregular particle interface within the scope of Fig. 5 (b) for the magnets doped with 1.0 wt.% $Cu_{10}Zn_{90}$ alloy powders. It is found that the regions marked by blue lines in the larger areas (Figs. 4a and 5a) served well as the basis for Fig. 3. Doping 1.0 wt.% Zn or $Cu_{10}Zn_{90}$ powders into sintered NdFeB magnets is beneficial for the "connection" of the regular/irregular particle interface during SPS, which is in good agreement with the SEM results mentioned above. Two factors can contribute to the "connection" effect in the sample: the liquid phase connection (physical connection) by doping low-melting powders into the interface, and the bond connection by the chemical reaction between the doping powders and the Nd-containing phase in melt-spun powders, which have been proved by the XRD results mentioned above. Moreover, Cu or Zn are evenly partitioned in the irregular particle interfaces of the magnets doped with 1.0 wt.% $Cu_{10}Zn_{90}$ powders from the EDS elemental maps shown in Fig. 5, indicating that the doping additives are distributed evenly before SPS.

Figure 6 shows the grain morphology in areas away from the interface for the sintered magnets doped with different powders additions. Compared with the additive-free magnets, the Zn- or $Dy_2O_3$-doped magnets have relatively small mean grain size, roughly 100 nm. It is, therefore, reasonable to consider that both additives play an important role in suppressing grain coarsening of $Nd_2Fe_{14}B$ phase during SPS.

Figure 7 shows the room-temperature demagnetization curves of the sintered magnets with different alloy additions. All the magnets exhibit smooth demagnetization curves when doping content is lower than 2.0 wt.%. Figure 8 describes the dependence of remanence $J_r$, intrinsic coercivity ${}_jH_c$, maximum energy product $(BH)_{max}$ and density on the doping content for sintered magnets with (a) Zn,

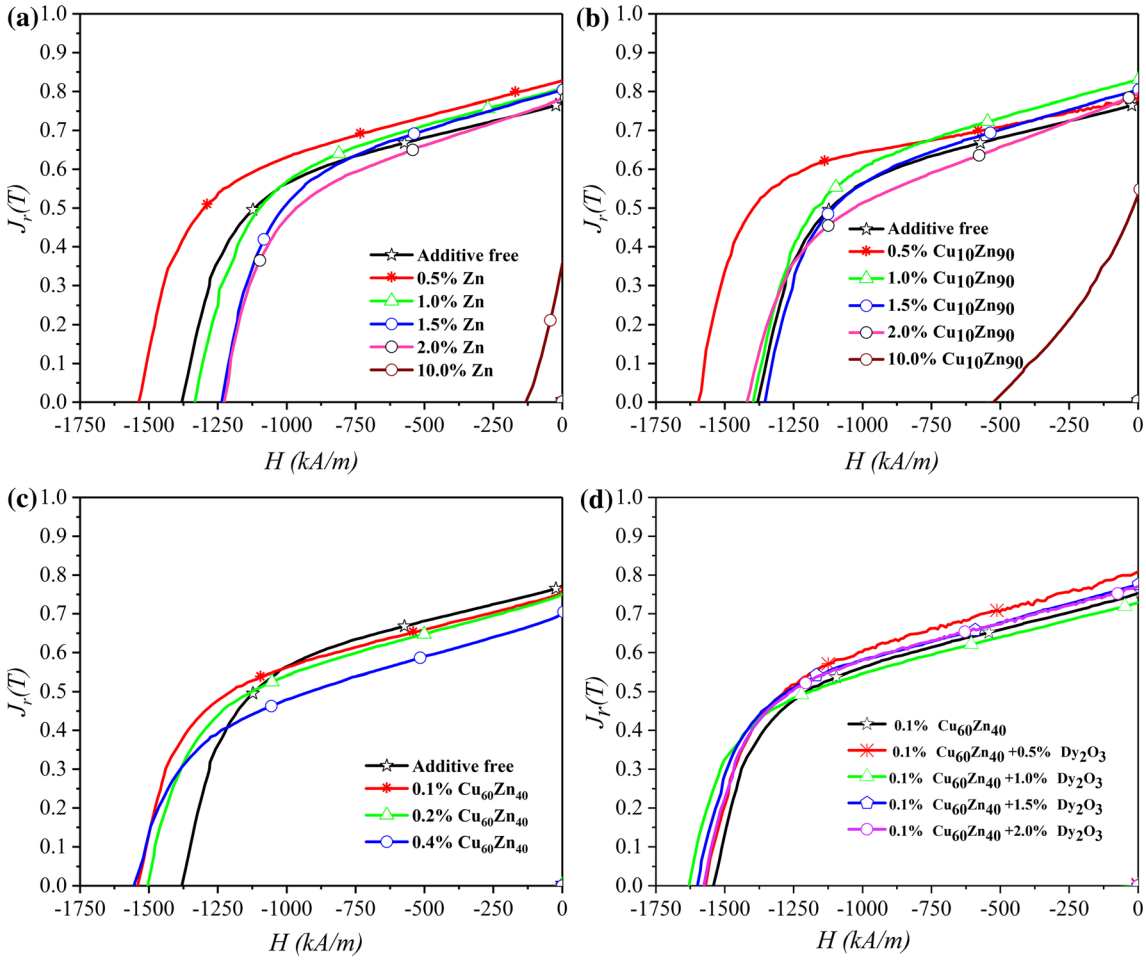


Fig. 7. Room temperature demagnetization curves for magnets added with various contents of (a) Zn, (b) $Cu_{10}Zn_{90}$, (c) $Cu_{60}Zn_{40}$, and (d) combined additions of 0.1 wt.% $Cu_{60}Zn_{40}$ + *x* wt.% $Dy_2O_3$.

(b) $Cu_{10}Zn_{90}$, (c) $Cu_{60}Zn_{40}$, (d) 0.1 wt.% $Cu_{60}Zn_{40}$ + *x* wt.% $Dy_2O_3$ additions. For the additive-free magnets, the magnetic properties of $J_r$= 0.77 T, ${}_jH_c$= 1381 kA/m, and $(BH)_{max}$ = 103 kJ/m$^3$ are obtained using a SPS pressure of 60 MPa. The value of ${}_jH_c$ enhanced to 1537 kA/m and 1596 kA/m by doping 0.5 wt.% Zn and 0.5 wt.% $Cu_{10}Zn_{90}$ alloy powders, respectively, with $(BH)_{max}$ slightly increased to 119 kJ/m$^3$ and 109 kJ/m$^3$ due to an increasing of $J_r$ to 0.83 T and 0.78 T, respectively, as shown in Fig. 8a and b. It is very exciting to obtain magnets with both higher ${}_jH_c$ and $(BH)_{max}$, because this is quite important for reducing the size of the magnetic devices. The further densification due to the "connection" effect and grain refinement effect can explain why the simultaneous enhancement of ${}_jH_c$ and $(BH)_{max}$ are obtained. In addition, the magnets doped with high contents of Zn or $Cu_{10}Zn_{90}$ (10.0 wt.%) show extremely low magnetic properties and the presence of a large amount of coarse grains formed by the chemical reaction heat[8] and the obvious reduced volume fraction of $Nd_2Fe_{14}B$ phase are responsible for the decrease.

The magnets doped with various contents of $Cu_{60}Zn_{40}$ powders were also prepared. From Fig. 8c, the value of ${}_jH_c$ enhanced to 1542 kA/m with a slight decrease of $J_r$ and $(BH)_{max}$ by doping 0.1 wt.% $Cu_{60}Zn_{40}$ alloy powders, which can be explained by the small amount of pores caused by a lower "connection" effect resulting from the relatively lower conductivity and higher melting point, compared with Zn or $Cu_{10}Zn_{90}$ alloy.

The ${}_jH_c$, $J_r$, actual density ($\rho_{actual}$), theoretical density ($\rho_{theoretical}$) for magnets sintered with different additions at room temperature are summarized in Table I and Table II. It is found that doping an optimized amount of alloy powders (except for the $Cu_{60}Zn_{40}$-doped magnets) into magnetic powders plays an important role in improving the densities of sintered magnets by comparing the $\rho_{actual}$ with the $\rho_{theoretical}$, in accordance with the results shown in Fig. 2. Doping 0.5 wt.% Zn, 0.5 wt.% $Cu_{10}Zn_{90}$ or 0.1 wt.% $Cu_{60}Zn_{40}$ powders can effectively enhance the value of ${}_jH_c$ by 11.3%, 15.6%, or 11.7%, respectively. For further enhancing the coercivity, selected magnets co-doped with low-cost $Dy_2O_3$ powders[25] were also studied. For the combined 0.1 wt.% $Cu_{60}Zn_{40}$ and 1.0 wt.% $Dy_2O_3$ -doped magnets, the magnetic properties of $J_r$= 0.71 T, ${}_jH_c$= 1630 kA/m, and $(BH)_{max}$ = 92 kJ/m$^3$ were

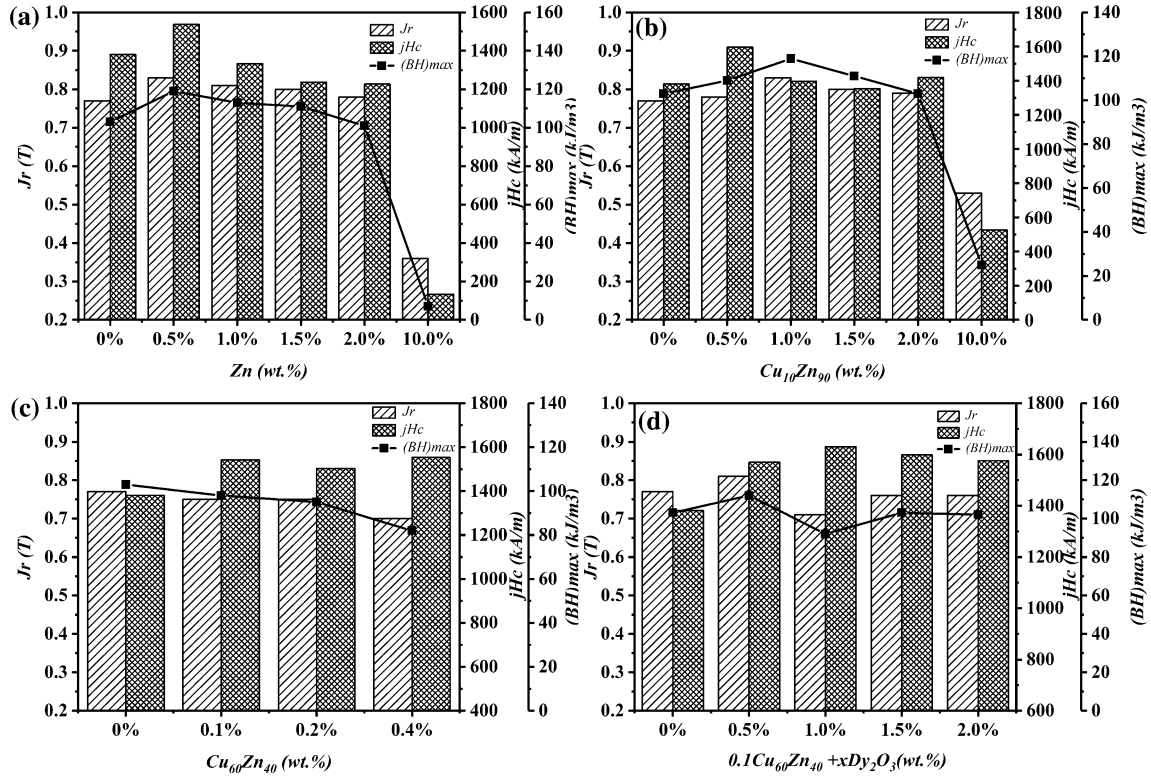


Fig. 8. Comparison of the magnetic properties and density of sintered magnets doped with different powders with different weight ratios: (a) Zn, (b) $Cu_{10}Zn_{90}$, (c) $Cu_{60}Zn_{40}$, (d) 0.1 wt.% $Cu_{60}Zn_{40}$ + *x* wt.% $Dy_2O_3$.

**Table I. $_jH_c$, $J_r$, actual density ($\rho_{actual}$), theoretical density ($\rho_{theoretical}$) for sintered magnets sintered with different Zn and $Cu_{10}Zn_{90}$ additions at room temperature**

| | Zn | | | | | $Cu_{10}Zn_{90}$ | | | |
|---|---|---|---|---|---|---|---|---|---|
| **Content (wt.%)** | **$_jH_c$ (kA/m)** | **$J_r$ (T)** | **$\rho_{actual}$ (g/cm$^3$)** | **$\rho_{theoretical}$ (g/cm$^3$)** | | **$_jH_c$ (kA/m)** | **$J_r$ (T)** | **$\rho_{actual}$ (g/cm$^3$)** | **$\rho_{theoretical}$ (g/cm$^3$)** |
| Additive-free (%) | 1381 | 0.77 | 7.39 | 7.531 | Additive-free (%) | 1381 | 0.77 | 7.39 | 7.531 |
| 0.5 | 1537 | 0.83 | 7.42 | 7.529 | 0.5 | 1596 | 0.78 | 7.41 | 7.530 |
| 1.0 | 1334 | 0.81 | 7.40 | 7.527 | 1.0 | 1397 | 0.83 | 7.44 | 7.529 |
| 1.5 | 1236 | 0.80 | 7.41 | 7.525 | 1.5 | 1354 | 0.80 | 7.40 | 7.528 |
| 2.0 | 1227 | 0.78 | 7.40 | 7.524 | 2.0 | 1419 | 0.79 | 7.40 | 7.527 |
| 10.0 | 133 | 0.36 | 6.97 | 7.494 | 10.0 | 525 | 0.53 | 7.02 | 7.510 |

**Table II. $_jH_c$, $J_r$, actual density ($\rho_{actual}$), theoretical density ($\rho_{theoretical}$) for sintered magnets sintered with different $Cu_{60}Zn_{40}$ and 0.1 wt.% $Cu_{60}Zn_{40}$ + *x* wt.% $Dy_2O_3$ additions at room temperature**

| | $Cu_{60}Zn_{40}$ | | | | 0.1 wt.% $Cu_{60}Zn_{40}$ + *x* wt.% $Dy_2O_3$ | | | | |
|---|---|---|---|---|---|---|---|---|---|
| **Content (wt.%)** | **$_jH_c$ (kA/m)** | **$J_r$ (T)** | **$\rho_{actual}$ (g/cm$^3$)** | **$\rho_{theoretical}$ (g/cm$^3$)** | ***x*= %** | **$_jH_c$ (kA/m)** | **$J_r$ (T)** | **$\rho_{actual}$ (g/cm$^3$)** | **$\rho_{theoretical}$ (g/cm$^3$)** |
| Additive-free (%) | 1381 | 0.77 | 7.39 | 7.531 | 0. 5 | 1570 | 0.81 | 7.40 | 7.533 |
| 0.1 | 1542 | 0.75 | 7.37 | 7.532 | 1.0 | 1630 | 0.71 | 7.42 | 7.535 |
| 0.2 | 1504 | 0.75 | 7.36 | 7.532 | 1.5 | 1599 | 0.78 | 7.39 | 7.536 |
| 0.4 | 1554 | 0.70 | 7.32 | 7.533 | 2.0 | 1576 | 0.77 | 7.40 | 7.537 |

obtained, as shown in Fig. 8d. Hence, an extra addition of proper amount of $Dy_2O_3$ powders (1.0 wt.%) is beneficial for further enhancing ${}_jH_c$ of $Cu_{60}Zn_{40}$-doped NdFeB magnets, in consistence with our previous study.[8]

## CONCLUSION

Nanocrystalline NdFeB magnets have been prepared by SPS using melt-spun $Nd_{10.15}Pr_{1.86}Fe_{80.41}Al_{1.67}B_{5.91}$ powders. Doping non-rare earth $Cu_xZn_{100-x}$ alloy powders and $Dy_2O_3$ powders have been proved to be a practical approach to enhance the properties of sintered NdFeB magnets. The results show that the density of the sintered NdFeB magnets can be further enhanced by doping Zn or $Cu_{10}Zn_{90}$ due to the "connection" effect at the particle interface during SPS. The EDS analysis showed that Cu and Zn are evenly partitioned in irregular particle interfaces in the $Cu_{10}Zn_{90}$-doped magnets, which contributes to the formation of fully dense magnets during SPS. Zn or $Dy_2O_3$ plays an important role in suppressing grain coarsening of $Nd_2Fe_{14}B$ phase during SPS. As a result, the magnetic properties, in particular, the coercivity, has been enhanced by the doping. The magnetic properties of the sintered magnets doped with 0.5 wt.% Zn, 0.5 wt.% $Cu_{10}Zn_{90}$ or 0.1 wt.% $Cu_{60}Zn_{40}$ are found to be very attractive. 0.5 wt.% Zn doped magnet has $J_r$= 0.83 T, ${}_jH_c$= 1537 kA/m, and $(BH)_{max}$ = 119 kJ/m$^3$. $J_r$= 0.78 T, ${}_jH_c$= 1596 kA/m, and $(BH)_{max}$ = 109 kJ/m$^3$ were obtained in 0.5 wt.% $Cu_{10}Zn_{90}$ doped magnet. $J_r$= 0.75 T, ${}_jH_c$= 1542 kA/m, and $(BH)_{max}$ = 98 kJ/m$^3$ were obtained in 0.1 wt.% $Cu_{60}Zn_{40}$ doped magnet. The magnets doped with 0.5 wt.% Zn or 0.5 wt.% $Cu_{10}Zn_{90}$ exhibited a higher ${}_jH_c$ with a slight increase in both $J_r$ and $(BH)_{max}$. Meanwhile, the extra addition of 1.0 wt.% $Dy_2O_3$ is helpful in further improvement of ${}_jH_c$ for 0.1 wt.% $Cu_{60}Zn_{40}$-doped NdFeB magnets.

## ACKNOWLEDGMENT

This work was supported by the Jiangxi Provincial Science and Technology Program (Grant No. GJJ171308), the National Natural Science Foundation of China (Grant No. 51774146), Guangzhou Municipal Science and Technology Program (No. 201707010161) and the Guangdong Key Laboratory of Rare Earth Development and Applications (Grant No. XTKY-201801).

## REFERENCES

1. O. Gutfleisch, M.A. Willard, E. Bruck, C.H. Chen, S.G. Sankar, and J.P. Liu, *Adv. Mater.* 23, 821 (2011).
2. K. Hirota, H. Nakamura, T. Minowa, and M. Honshima, *IEEE Trans. Mag.* 42, 2909 (2006).
3. Q. Zhou, Z.W. Liu, X.C. Zhong, and G.Q. Zhang, *Mater. Des.* 86, 114 (2015).
4. H.X. Zeng, Z.W. Liu, W. Li, J.S. Zhang, L.Z. Zhao, X.C. Zhong, H.Y. Yu, and B.C. Guo, *J. Magn. Magn. Mater.* 471, 97 (2019).
5. H. Sepehri-Amin, T. Ohkubo, and K. Hono, *Acta Mater.* 61, 1982 (2013).
6. N. Oono, M. Sagawa, R. Kasada, H. Matsui, and A. Kimura, *J. Magn. Magn. Mater.* 323, 297 (2011).
7. W. Chen, Y.L. Huang, J.M. Luo, Y.H. Hou, X.J. Ge, Y.W. Guan, Z.W. Liu, Z.C. Zhong, and G.P. Wang, *J. Magn. Magn. Mater.* 476, 134 (2019).
8. Z.W. Liu, L.Z. Zhao, S.L. Hu, H.Y. Yu, X.C. Zhong, and X.X. Gao, *IEEE Trans. Mag.* 51, 2101204 (2015).
9. F. Xu, L.T. Zhang, X.P. Dong, Q.Z. Liu, and M. Komuro, *Scr. Mater.* 64, 1137 (2011).
10. H. Nakamura, K. Hirota, T. Minowa, and M. Honshima, *IEEE Trans. Mag.* 41, 3844 (2005).
11. Q.Z. Liu, L.T. Zhang, X.P. Dong, F. Xu, and M. Komuro, *Scr. Mater.* 61, 1048 (2009).
12. Y.L. Ma, Y. Liu, J. Li, C.Y. Li, and L.H. Chu, *J. Magn. Magn. Mater.* 322, 2419 (2010).
13. W.J. Mo, L.T. Zhang, A.D. Shan, L.J. Cao, J.S. Wu, and M. Komuro, *Intermetallics* 15, 1483 (2007).
14. Y.L. Huang, Z.W. Liu, X.C. Zhong, H.Y. Yu, and D.C. Zeng, *Powder Metall.* 55, 124 (2012).
15. Z. Peng, D.Q. He, X. Mu, H.Y. Zhou, C.C. Li, S.F. Ma, P.X. Ji, W.K. Hou, P. Wei, W.T. Zhu, X.L. Nie, and W.Y. Zhao, *J. Electron. Mater.* 47, 3350 (2018).
16. Y. Liu, G.W. Xu, Y.Y. Xie, H. Lv, C.Y. Huang, Y.W. Chen, Z.F. Tong, J. Shi, and R. Xiong, *Ceram. Int.* 44, 9649 (2018).
17. M.A. Auger, Y. Huang, H. Zhang, C.A. Jones, Z. Hong, M.P. Moody, S.G. Roberts, and P.S. Grant, *J. Alloys Compd.* 762, 678 (2018).
18. P.Q. Zhao, Q.G. Li, R.J. Yi, Z. Wang, L.C. Lu, X. Cheng, and S.M. Dong, *J. Alloys Compd.* 748, 36 (2018).
19. Z.B. Yin, J.T. Yuan, W.W. Xu, K. Liu, and S.Y. Yan, *Ceram. Int.* 44, 8977 (2018).
20. X.X. Li, C. Yang, T. Chen, Z.Q. Fu, Y.Y. Li, O.M. Ivasishin, and E.J. Lavernia, *Scr. Mater.* 151, 47 (2018).
21. T.N. Maity, K. Biswas, and B. Basu, *Acta Mater.* 152, 215 (2018).
22. M. Galatanu, M. Enculescu, and A. Galatanu, *Mater. Res. Express.* 5, 026502 (2018).
23. Z.W. Liu, H.Y. Huang, X.X. Gao, H.Y. Yu, X.C. Zhong, J. Zhu, and D.C. Zeng, *J. Phys. D Appl. Phys.* 44, 025003 (2011).
24. Y.L. Huang, Z.W. Liu, X.C. Zhong, and H.Y. Yu, *J. Appl. Phys.* 111, 033913 (2012).
25. K.H. Bae, T.H. Kim, S.R. Lee, and S. Namkung, *J. Appl. Phys.* 112, 093912 (2012).